

Nanoscale

Accepted Manuscript



This is an *Accepted Manuscript*, which has been through the Royal Society of Chemistry peer review process and has been accepted for publication.

Accepted Manuscripts are published online shortly after acceptance, before technical editing, formatting and proof reading. Using this free service, authors can make their results available to the community, in citable form, before we publish the edited article. We will replace this *Accepted Manuscript* with the edited and formatted *Advance Article* as soon as it is available.

You can find more information about *Accepted Manuscripts* in the [Information for Authors](#).

Please note that technical editing may introduce minor changes to the text and/or graphics, which may alter content. The journal's standard [Terms & Conditions](#) and the [Ethical guidelines](#) still apply. In no event shall the Royal Society of Chemistry be held responsible for any errors or omissions in this *Accepted Manuscript* or any consequences arising from the use of any information it contains.



Journal Name

ARTICLE

Au modified three-dimensional In_2O_3 inverse opals: synthesis and improved performance for acetone sensing toward diagnosis of diabetes

Received 00th January 20xx,
Accepted 00th January 20xx

DOI: 10.1039/x0xx00000x

www.rsc.org/

Key words: In_2O_3 , Au, gas sensing, inverse opal, exhaled breath

Ruiqing Xing, Qingling Li, Lei Xia, Jian Song, Lin Xu*, Jiahuan Zhang, Yi Xie, and Hongwei Song*

Analyzing the volatile organic compounds (VOCs) in exhaled breath effectively is crucial to the medical treatment, which can provide a fast and noninvasive way to diagnose disease. Well-designed materials with controlled structures have great influence on the sensing performance. In this work, the ordered three dimensional inverse opal (3DIO) macroporous In_2O_3 films with additional *via* holes architectures were fabricated and different amounts of gold nanoparticles (Au NPs) were loaded on the In_2O_3 films aiming at enhancing their electrical responses. The gas sensing to acetone toward diabetes diagnosis in exhaled breath was performed through different Au/ In_2O_3 electrodes. Representatively, the best 3DIO Au/ In_2O_3 sensor can detect acetone effectively at 340°C with response of 42.4 to 5 ppm, the actual detection limit is as low as 20 ppb, and it holds the dynamic response of 11 s and a good selectivity. Moreover, the clinic test proved that as-prepared 3DIO Au/ In_2O_3 IO sensor could distinguish the acetone biomarkers in human breath clearly. The excellent gas sensing properties for Au/ In_2O_3 electrodes were attributed to the “spillover effects” between Au and In_2O_3 and the special 3DIO structure. This work indicates that 3DIO Au/ In_2O_3 composite is a promising electrode material to actual application in monitoring and detecting diabetes through exhaled breath.

1. Introduction

Disease diagnosis using specific VOCs in exhaled breath has attracted so much attention because of its key advantages in terms of noninvasive, real-time, and potentially inexpensive diagnosis.¹⁻⁴ Among these VOCs, acetone gas has been identified as a specific biomarker to the field of diabetes, clinical data shows that the concentration of exhaled acetone from diabetes exceed 1.8 ppm, while for healthy people is only 0.3–0.9 ppm. Thus, many ways have been developed to breathe analysis for potential diabetes detection.^{3, 5} Among these methods, oxide-semiconductor gas sensors possess the advantages of superior reaction with VOCs, easy fabrication, high miniaturization potential, and possibility of integration in portable devices. However, because of the complicated environment in exhaled breath (ppb level VOCs, highly humid atmospheres, and etc.), an ideal gas sensor for exhaled VOCs analysis should be sensitive to very low analytic concentrations in the presence of water vapor, respond rapidly to small changes in concentration, and provide a consistent output which is specific to a given exposure.⁶ Thus, the fabrication of the

gas sensor for exhaled VOCs analysis that can meet clinical requirements remains a challenge.

It is known that the sensing performances of oxide-semiconductor gas sensors depend on the interaction between the testing gas molecules and the adsorbed oxygen molecules on the surface of sensing films. Thus, the microstructural parameters of the film including pore size, surface area, porosity, and film thickness have great influence on the properties of the sensors.^{7, 8} Being a special kind of nanostructure, 3DIO nanomaterials provide a new approach to the design and fabrication of novel sensors via their special manipulation properties. Such 3DIO materials have high degree of well-ordered porous architecture as well as easily controlled pore size, which can increase and regulate the effective surface area of sensing materials to the target gases, and make the electrons transport quickly.^{9, 10} Besides, the 3DIO nanostructure also provides high gas accessibility that let analyses gas molecules access readily and quickly.¹¹ All these merits improve the gas sensing properties effectively, for instance, Arienzo et al prepared WO_3 , Cr-doped and Pt-doped 3DIO NH_3 sensors and Qzin et al. applied SnO_2 3DIO sensors to the detection of CO gas.^{9, 12} However, the application of 3DIO sensors on exhaled VOCs sensing is quite rare. Previously, we fabricated a series of 3DIO ZnO-CuO sensors which showed good performance to diabetes biomarker (acetone, 0.1–50 ppm) even under quite high humidity, indicating the 3DIO oxide-

State Key Laboratory on Integrated Optoelectronics, College of Electronic Science and Engineering, Jilin University, Changchun, 130012, People's Republic of China.
*E-mail: linxu@jlu.edu.cn, songhw@jlu.edu.cn Tel: 86-431-81736604

semiconductor electrode is a promising device to exhaled breath sensing.¹³ Recently, Lee et al. synthesized a monolayer α - Fe_2O_3 IO film with additional *via* holes, which was proved to be effective in detecting trace levels of NO_2 gas in a timely and sensitive manner.¹⁴ However, compared to 3D structure, such monolayer limits the effective surface area of the sensitive material.

In this work, we represent our recent progresses in the controlled fabrication of ordered 3DIO macroporous films with regular honeycomb-like morphology, highly homogenous layout, 3DIO skeleton with additional orderly *via* holes. In_2O_3 was chosen as model materials, which had been widely used for the gas detection due to its excellent electrical properties.¹⁵⁻¹⁸ Besides, different amount of Au NPs were loaded on the 3DIO In_2O_3 macroporous films ($\text{Au}/\text{In}_2\text{O}_3$) uniformly to further enhance its sensing properties. Here, Au NPs were chosen as catalyst of the surface reaction and specific adsorption sites for oxygen, due to its better thermal stability than Ag and much lower cost than Pt or Pd. Moreover, we observed that the 3DIO $\text{Au}/\text{In}_2\text{O}_3$ films demonstrated excellent sensing permanence to trace acetone gas, which is an important biomarker in exhaled breath to diabetes diagnoses.

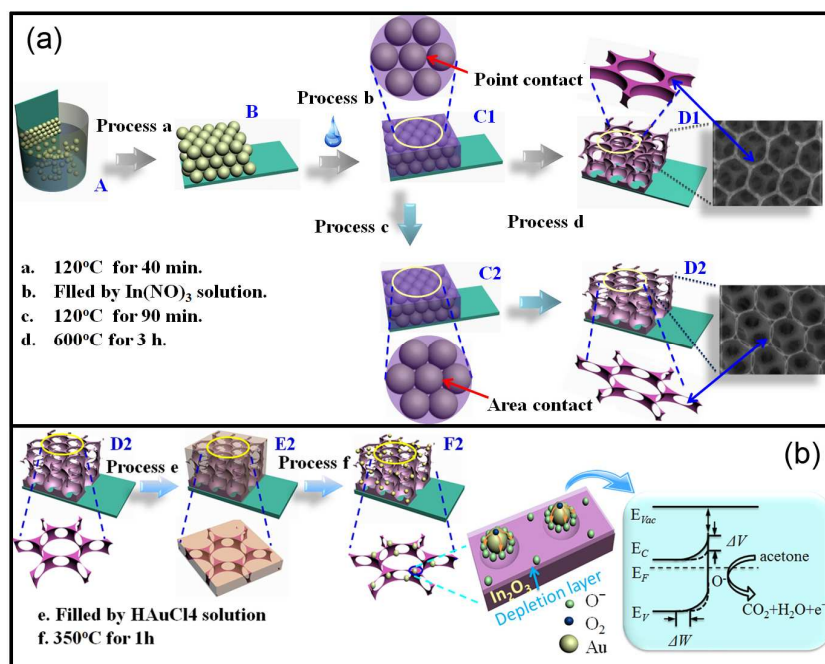
2. Experimental section

2.1 Materials and equipment

Mono-dispersed polymethyl methacrylate (PMMA) spheres were synthesized by methyl methacrylate in our laboratory.¹⁹ Indium

nitrate ($\text{In}(\text{NO}_3)_3 \cdot 4.5\text{H}_2\text{O}$) was bought from Sinpharm chemical reagent company (Shanghai, China). Citric acid and gold chloride (HAuCl_4) were bought from Tianjin Kaitong Company (Shanghai, China) and Tianjin guangfu fine research institute, respectively. Ethanol and sulfuric acid (98%) were bought from Beijing Chemical Works (Beijing, China). All the chemicals used in this work were analytical grade and without further purification. Slide glasses were the products by Shanghai Glass, Inc. (Shanghai, China). Deionized water ($>18 \text{ M}\Omega$) was used for the experiments.

The morphology of the samples was inspected using a JEOL JSM-7500F (Japan) field emission scanning electron microscope (SEM) with accelerating voltage of 15 kV and gold sputtering on the surface. Transmission electron microscope (TEM) and high resolution TEM (HRTEM) images were recorded on a JEM-2010 transmission electron microscope under a working voltage of 200 kV. The phase structure of the samples were characterized by X-ray diffraction (XRD), and the XRD patterns were conducted on Rigaku D/max 2550 using a mono-chromatized Cu target radiation resource ($\lambda=1.5045 \text{ \AA}$) and corresponding lattice constants were calculated by MDI Jade 5.0 software. X-ray photoelectron spectroscopy (XPS) was conducted on an ESCALab250 Analytical XPL Spectrometer with a monochromatic Al KR source. All the binding energies were referred to the C1s peak at 284.7 eV of the surface adventitious carbon. The fitted peaks in XPS spectra were deconvoluted using the XPS Peak 4.1 software. Working function values of the samples were measured by Kelvin Probe SKP5050 system made in England.



Scheme 1 The schematic view of process to fabricate (a) 3DIO In_2O_3 films with an improved macroporous structure and (b) Au loaded 3DIO In_2O_3 films. The right part of panel b is schematic view of the two major processes taking place at 3DIO $\text{Au}/\text{In}_2\text{O}_3$ films: adsorption and dissociation of oxygen at the regions close to $\text{Au}/\text{In}_2\text{O}_3$ interface and adsorption of oxygen on pure In_2O_3 . And the energy band schematic diagram of 3DIO $\text{Au}/\text{In}_2\text{O}_3$, the depletion layer at the regions close to the $\text{Au}/\text{In}_2\text{O}_3$ interface (solid line) is wider (ΔW) and higher (ΔV) than that at the pristine In_2O_3 surface (dashed line).



Journal Name

ARTICLE

2.2 Fabrication of 3DIO Au/In₂O₃ films with improved nanostructure

The fabrication process of the 3DIO films is shown in Scheme 1a. The typical process to obtain the common 3DIO structure is similar to the method reported previously, as briefly described in process A→B→C1→D1.¹³ For the improved structure with additional *via* holes, the monodisperse PMMA spheres were first self-assembled on a cleaned glass substrate through the vertical deposition process, and this process is the same with the common one. Then the substrate was sintered to the temperature of 120°C which is near to the glass-transition temperature of PMMA for 40 min (process a, to obtain status B), to reduce the distance between the PMMA spheres and enhance its physical strength of the PMMA opal array. Subsequently, the interstitial spaces between the PMMA spheres were filled by 0.76 M In(NO₃)₃ solution (in ethanol) containing 0.26 M citric acid (process b, to obtain status C1). Here, the citric acid plays a role as complexing agent to adjust the solution viscosity and surface tension. Then the filled samples were placed in an oven with 120°C for 90 min to further close the distance between the PMMA spheres, and then the point contact between the adjacent spheres to area contact was changed (process c, to obtain status C2).²⁰ Note that this process is essential for the formation of the improved 3DIO nanostructure with additional *via* holes and in this process the solution on the surface will evaporate a little. Finally, the films were annealed in a tube furnace with a speed of 1°C/min to 600°C for 3 h to remove the polymer spheres completely and solidify the network and then self-cooled down to room temperature naturally (process d). Finally, the 3DIO In₂O₃ films with improved nanostructure were obtained (status D2). In our previous work, we found that the 3DIO films showed different gas sensing properties towards tracing methanal gas due to the different pore size.²¹ Thus, two 3DIO In₂O₃ films with different pore sizes were prepared, by using ~295 nm and 585 nm PMMA spheres as templates, and they were named as S1 and S2, respectively.

As illustrate in Scheme 1b, 3DIO Au/In₂O₃ films was obtained through wetting the improved 3DIO In₂O₃ films (S2) by 50 mM HAuCl₄ solution (in deionized water) and then dried at room temperature for 30 min (process e, to obtain status E1). The films modified with various volumes HAuCl₄ solution was obtained by repeating this immerse procedure for one (S3), three (S4) and seven times (S5), respectively. Then, the films loading with different amount of HAuCl₄ were annealed at 350°C for 1 h at a heating rate of 1°C/min to tune HAuCl₄ to Au NPs (process f, to obtain status F2). Finally, the improved 3DIO Au/In₂O₃ films were obtained.

2.3 Fabrication and measurement of as-fabricated gas sensor

To fabricate the corresponding 3DIO gas sensors, 3DIO films were first scraped down from the glass substrates and then mixed with ethanol in a weight ratio of 5:1 to form a paste, the paste was coated onto an alumina tube on which a pair of gold electrodes was previously printed. A Ni–Cr alloy coil was inserted into the alumina tube to provide the operating temperature. After the solvent was evaporated, the ceramic tube coated with samples thin layer was sintered in an oven for 1 h at 200°C. After sintering, the gas sensors were thermal aged with a heating voltage of 4.25 V at the ageing equipment for 3 h before the first measurement.

The gas-sensing properties were measured on a WS-30A system (Weisheng Instruments Co., Zhengzhou, China) and determined under laboratory conditions (22±2 RH%, 20±2°C). During the experiment the constant measurement voltage was 5 V. Here, a static liquid gas distribution method was used to achieve different gas volume fractions of the target gases. The gas sources were 1000 ppm standard gas mixed with N₂. During testing, a certain amount of standard gas was injected into the glass chamber through a small mouth (about 2.5 L in volume) which had been pumped in a vacuum state and then mixed with the ambient gas. Both the inner wall of the mouth and the corresponding rubber stopper were sealed by petroleum jelly in order to maintain the stability of the gas concentration. In this process, the sensor with an extended line went through the rubber stopper was put into the chamber, when the response reached a constant value, the sensor was taken out to recover in ambient air. The response is defined as R_a/R_g for n-type sensor where R_a and R_g are the resistance for sensors in air and in target gas, respectively. The response and recovery times are defined as the time required to reach 90% of the final equilibrium value.

The dehumidification treatment in this work is represented in Scheme S1. First, the human exhaled breath with RH value nearly 100% (measured by a precise hygrometer, Hcjyjet, HT-635) was collected into a gas collecting bag with aluminum coating, and then the gas in the bag was pumped out by an air pump through a drying tube which filled by silica gels and molecular sieves desiccant. Finally the gas was collected into another gas collecting bag. By this way the RH value in exhaled breath can be reduced to 20%.

3. Results and discussion

3.1 Morphologies and structure properties of samples

The morphology and microstructure of the as prepared 3DIO films with improving structures are investigated in Fig. 1. For the pure In₂O₃ IO samples, it can be seen that all the samples yield a long-range ordered hexagonal arrangement of IO nanostructure. Besides, comparing to the common In₂O₃ 3DIO structure (Scheme 1, status D1), the side walls of the as prepared In₂O₃ IO samples with improving structure display additional *via* holes, which can be

assigned to the increase in contact area between two adjacent PMMA spheres (from point contact to area contact) by softening the template sphere at 120 °C.¹⁴ Note that the marked arrows in the status C1 and C2 of Scheme 1 reveal a more clearly comparison of the difference between two structures. For the S1 and S2 samples, the pore sizes are determined to be ~180 nm (Fig. 1a) and 420 nm (Fig. 1b), respectively, due to the different PMMA template diameter. And their colours under normal indoor environment are both light yellow (Fig. S1a and b), however, the color of S2 sample seems a little darker because the different pore size lead to different band gap position. Fig. 1c gives an enlarged SEM image of S2 samples, because of the closer distance between the adjacent PMMA spheres, the skeleton of the 3DIO In₂O₃ films is quiet thick which is about ~13.5 nm (as the arrow pointed). Note that due to the influence of gravity and the squeezing effect between the neighbouring frames, it is hard for *via* holes structures to keep the vertical state.

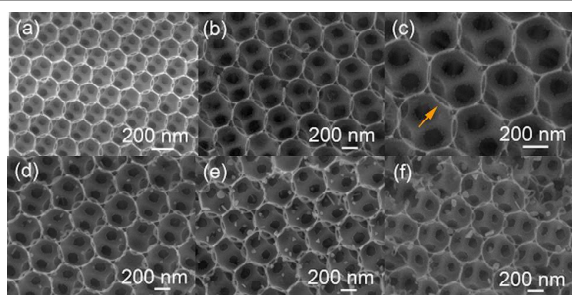


Fig. 1 (a-b) SEM images of (a) S1 and (b) S2 3DIO In₂O₃ films. (c) The enlarged SEM of Fig 1b. (d-f) SEM images of S3-S5 3DIO Au/In₂O₃ films.

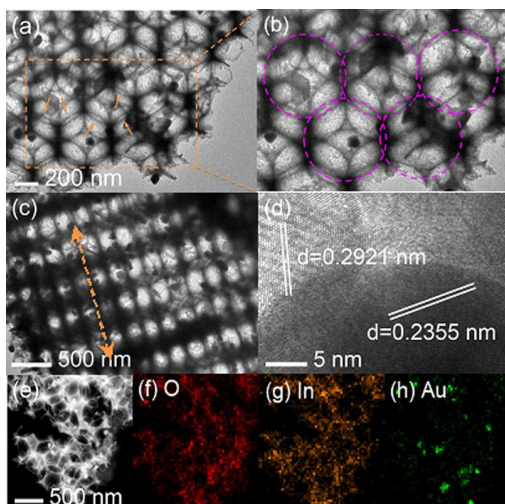


Fig. 2 TEM images of (a) S4 Au/In₂O₃ sample, (b) the enlarged image of Fig. 2a, and (c) TEM of S4 Au/In₂O₃ sample from side view. The arrows in panel are pointed to the *via* holes, and in panel c is point out the direction from face to substrate. (d) HR-TEM image of S4 Au/In₂O₃ sample. (e-h) EDX elemental mapping images of O, In, and Au of S4 Au/In₂O₃ sample.

For the 3DIO films loading with different amount of Au NPs, the corresponding Au NPs are dispersed uniformly. At first, a few

Au NPs can be observed after once immersing in HAuCl₄ solution for in S3 3DIO sample (Fig. 1d), and the colour of the film changes obviously from light yellow to light purple which is the feature colour of Au in nanoscale (Fig. S1d). Then the loading amount increases obviously after immersing in HAuCl₄ solution for three times (S4, Fig. 1e) and the corresponding colour also become darker (Fig. S1e). However, when further increased the immersed time (S5, seven times, Fig. 1f), the Au NPs size will become larger instead of quantity increase while the 3DIO structure will also be destroyed in some extent, thus the corresponding colour turn to golden (Fig. S1f).

TEM images can show the architectural detail in another perspective. Fig. 2a and 2b are the vertical view of S4 Au/In₂O₃ sample, the *via* hole structure and the loading Au NPs can be clearly seen, as the arrows point. In Fig. 2b, the specific structure of as fabricated S4 Au/In₂O₃ sample was highlight by some dashed circles. Furthermore, from the side view of S4 Au/In₂O₃ sample, it is proved that the Au NPs not only exist on the IO surface, but loading on the whole 3DIO structure uniformly. Besides, the Au NPs size distribution in different Au/In₂O₃ samples were given in Fig. S2, which was calculated through measuring at least 100 Au NPs. Accordingly, average sizes of Au NPs in S3 and S4 Au/In₂O₃ samples are both ~36 nm, while the average size of Au NPs in S5 Au/In₂O₃ sample is ~65 nm. Besides, from the HRTEM image, the Au and In₂O₃ nanocrystals with interplanar distances of 0.24 nm and 0.29 nm, which are corresponding to (111) plane of face-cubic Au and (222) plane of body-cubic In₂O₃ respectively, can also be clearly observed, implying the formation of small Au NPs on the surface of substrate In₂O₃. To further determine the specific distribution of O, In, and Au elements, EDX mappings of S4 Au/In₂O₃ sample were conducted, as shown in Fig. 2e-h. It can be clearly seen that the distribution of O and In elements (Fig. 2f and 2g) is homogeneous and consists with the STEM image (Fig. 2e), the corresponding location of O matches well with that of In and does not change with the distribution of Au, indicating the uniform distribution of In₂O₃ in 3DIO skeleton. Moreover, the distribution of Au mainly disperses on the skeleton and aggregates to form NPs.

The crystallographic structure of the as-prepared 3DIO In₂O₃ as well as Au/In₂O₃ samples were examined by XRD, as illustrated in Fig. 3. All the samples are well-crystallized. For pure In₂O₃ samples (S1 and S2), the change of pore size has no impact on the XRD patterns. All the detectable patterns can be assigned to body-centered cubic In₂O₃ (JCPDS card no.06-0416). With increasing the amount of Au loading, the peak intensity of face-centered cubic Au (JCPDS card no.04-0784) gradually becomes distinct from S3 to S4, indicating the formation of Au/In₂O₃ composites. There are no obvious difference between the peak intensities for S4 and S5.

3.2 XPS

In order to further demonstrate the chemical composition and binding energy of the as-prepared 3DIO samples, XPS spectra were performed and compared. First, the complete spectra of all the samples are shown in Fig. 4a, which confirm the presence of In, O, C or Au atoms elements. In addition, based on XPS spectra, the atom ratios of Au/In have been quantitatively calculated to be 0.8, 2.1, and 3.0 at.% corresponding to the S3-S5 samples, respectively. These

atoms elements are all consistent with the above XRD and TEM results. Accordingly, the corresponding O 1s XPS spectra are enlarged in Fig. 4b. It can be seen that the O 1s core level electrons of all the studied 3DIO samples can be deconvoluted into three separate peaks, which can be assigned to different kinds of oxygen species: crystal lattice oxygen, deficient oxygen and the adsorbed oxygen species or OH groups, respectively, from low to high binding energy. Because of the different chemical environments of O in each IO samples, the corresponding characteristic peaks also have some shifts, especially after loading with Au NPs on the surface. Accordingly, the deficient oxygen ratios can be calculated through the integral area ratio of deficient oxygen peak area to total O1s peak.²² The corresponding deficient oxygen ratios in S1-S5 IO sensors are calculated to be 19.6%, 20.6%, 25.8%, 28.1% and 21.9%, respectively. For pure IO In_2O_3 samples, S2 can provide more deficient oxygen on the surface due to larger pore size. Besides, the amount of deficient oxygen of the $\text{Au}/\text{In}_2\text{O}_3$ IO samples (S3-S5) increases in comparison to pure IO In_2O_3 samples because of the well-known spillover effect.^{23, 24} Specially, S4 $\text{Au}/\text{In}_2\text{O}_3$ sample has the maximum amount of deficient oxygen, suggesting that more surface oxygen vacancies are formed on the surface of In_2O_3 samples.

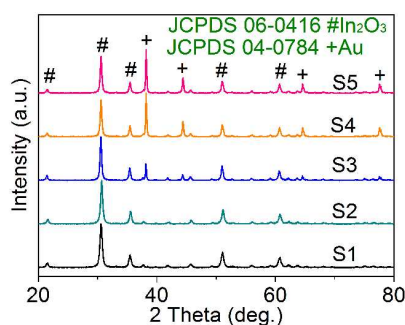


Fig. 3 XRD patterns of S1-S5 3DIO samples

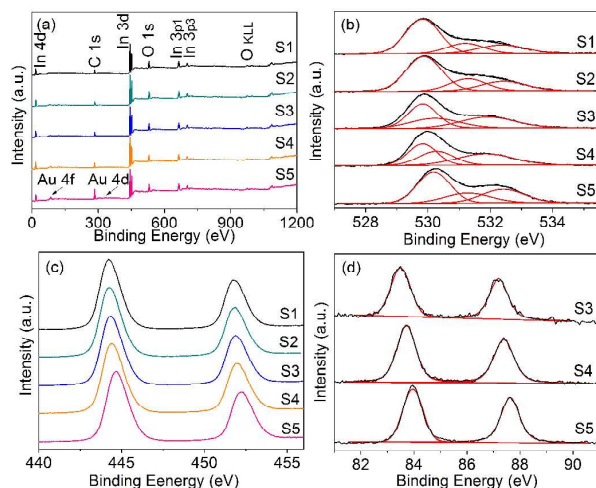


Fig. 4 (a) Survey, (b) O 1s, (c) In 3d high resolution XPS spectra of S1-S5 3DIO samples, and (d) Au 4f high resolution XPS spectra of S3-S5 3DIO $\text{Au}/\text{In}_2\text{O}_3$ samples.

The high resolution XPS spectra of In 3d are shown in Fig. 4c. All the 3DIO samples show two symmetric peaks, with binding energies around 444.2 eV and 451.7 eV, originating from $\text{In } 3d_{5/2}$ and $\text{In } 3d_{3/2}$, respectively. Comparing to pure 3DIO In_2O_3 samples, the In 3d peaks of $\text{Au}/\text{In}_2\text{O}_3$ IO samples (S3-S5) gradually shift to high binding energy side obviously with increasing amount of loaded Au NPs. Moreover, the similar shift also can be seen in the core level region of Au 4f spectra of S3-S5 samples (Fig. 4d). Note that XPS peaks indicate that the Au NPs in the studied samples all present the Au^0 state, which is consistent with the XRD analysis.

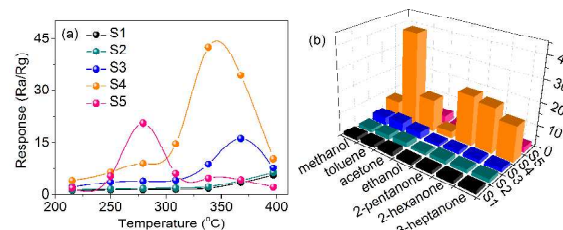


Fig. 5 (a) Responses of S1-S5 3DIO gas sensors to 5 ppm gaseous acetone as a function of operating temperature. (b) Selective tests of S1-S5 3DIO gas sensors for 5 ppm toluene, ethanol, methanol, 2-hexanone, 2-pentanone and 3-heptanone at 340°C.

3.3 Gas sensing properties of 3DIO In_2O_3 and $\text{Au}/\text{In}_2\text{O}_3$ sensors to exhale breath

3DIO nanostructures were expected to exhibit high gas sensitivity to low concentration target gas owing to the high surface area, well-order porous architecture as well as easily controlled pore size. Thus the gas sensing properties of 3DIO $\text{Au}/\text{In}_2\text{O}_3$ sensors compared with that of pure In_2O_3 sensors were investigated carefully towards trace acetone. It is known that the sensor response is largely influenced by its operating temperature. Accordingly, the sensor responses towards 5 ppm gaseous acetone were first examined as a function of operating temperature. As can be seen in Fig. 5a, the responses increase with temperature first and reach to a maximum value, and then some responses decrease with further increasing of the work temperature in the studied range. At low working temperature, the active sites amount on the semiconductor surface is rare, and thus the amount of adsorbed oxygen ions is deficient, leading to the poor response. With increasing the working temperature, the ion sorption of oxygen active sites amount will quickly increase, leading to improved response. While further increasing the working temperature, the surface gas may acquire enough kinetic energy to escape, lead to increase of the desorption process, and then make the amount of adsorbed oxygen ions decrease, which could lead to response deteriorate at higher temperature.^{25, 26} Besides, the pure 3DIO In_2O_3 sensor with larger pore size (S2) exhibits a little higher response than the smaller one (S1), while the pore size nearly has no influence on operating temperature, which is consistent with our previous work.²¹ For 3DIO $\text{Au}/\text{In}_2\text{O}_3$ sensors, both the optimum working temperature and effective response of the sensors are influenced by the loading

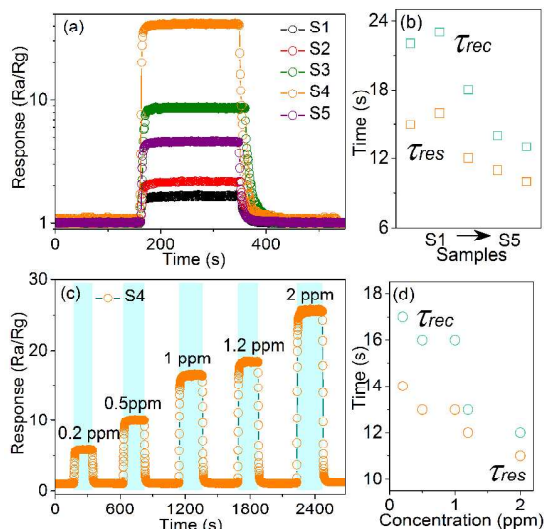


Fig. 6 (a) Dynamic responses of S1-S5 3DIO gas sensors to 5 ppm acetone at 340°C and (b) their corresponding response (τ_{res}) and recovery (τ_{rec}) times. (c) Dynamic responses of S4 Au/In₂O₃ gas sensor to different acetone concentrations at 340°C and (d) its corresponding response and recovery times.

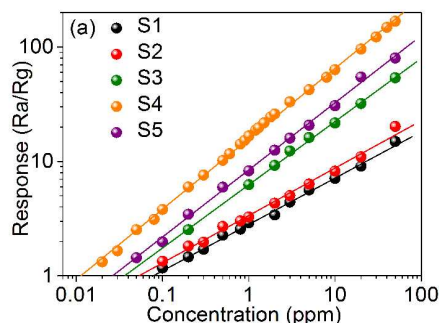


Fig. 7 The response curves of S1-S5 3DIO gas sensors to different acetone concentrations (20 ppb–50 ppm) at their corresponding optimal operating temperature.

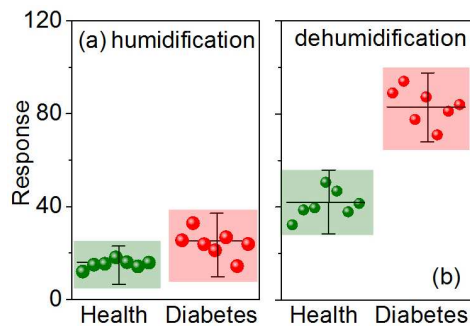


Fig. 8 The clinic tests response of S4 Au/In₂O₃ sensor to human breath: (a) direct collection and (b) after the dehumidification process.

amount of Au NPs. The optimal working temperature and response for S3-S5 3DIO Au/In₂O₃ sensors are 370°C and 16.1, 340°C and 42.4, and 280°C and 20.7, compared to pure In₂O₃ IO sensors (400°C and 5.6 for S1, 400°C and 6.3 for S2), respectively. As can be clearly seen, the optimal working temperature decreases gradually as increasing the content of surface Au NPs, and all the 3DIO Au/In₂O₃ sensors demonstrate an improved response in comparison to pure In₂O₃ gas sensors. Especially, compared to S2 In₂O₃ sensor, the response of S4 Au/In₂O₃ sensor improves ~6.7 times, while the working temperature decreases 60°C.

Selectivity is another important parameter for gas sensor in practical use, all the 3DIO sensors are further tested in various gases at 340°C to examine the selective properties and the interface gases including ethanol for drunk driving and toluene, methanol, 2-hexanone, 2-pentanone and 3-heptanone to lung cancer (all the gas concentrations are 5 ppm). As can be seen in Fig. 5b, the S4 Au/In₂O₃ sensor exhibits the highest response to all the test gases at 340°C, especially to acetone, whereas the other 3DIO sensors only have much lower response at the same temperature. Moreover, the responses of the sensors to ketones were higher than other gases. Generally, due to chemical bond types, molecular size and the molecular structure were different, each kind of gas has its optimum temperature due to different interaction between the gas and the sensor material. Thus, selecting a fixed temperature is an effective way that can maximize sensitivity to a particular analytic gas.^{25,27} As demonstrated in Fig. S3, we provide the response curves of some VOCs depending on temperature in Fig. 5b to further clarify the selectivity. The results show that other gases also demonstrate better responses at their optimum temperatures, while at 340°C, their responses become lower. Besides, we can see that the optimal working temperatures are much closer in ketones, that's the reason why the responses are higher than the other gases, however, the corresponding responses still have big difference. Note that because the effect factors to the response of a semiconductor sensor in the presence of target gases are very complex, the origin mechanism is still not very clear now, which will be an important future task.

The response transients of different 3DIO sensors exposed to 5 ppm acetone gas at 340°C are shown in Fig. 6a. As depicted, the responses of all the sensors exhibit drastic rises when exposed to acetone gas and quick drop to their initial states after the sensors are placed in the air ambient. Based on Fig. 6a, the response times and recovery times are calculated and shown in Fig. 6b. The data shows that the change of pore size has little effect on the dynamic times, however, the response times and recovery times gradually decrease with the increasing amount of loading Au NPs due to its catalytic action. Based on the above gas sensing characteristic analysis, S4 Au/In₂O₃ sensor is the optimum for acetone detection, thus further investigation would focus on it. Fig. 6c exhibits the dynamic response curves of S4 Au/In₂O₃ sensor to 0.2-2 ppm acetone, since 1.8 ppm is the healthy alert thresholds for diabetes.²⁸ It is apparent that the sensor has quick response when exposed to very low acetone concentration, and the response increases with the increasing of acetone concentration. Note that the sensor exhibits high response to acetone even at low concentrations. The corresponding response values can reach 6.0 and 18.7 to 0.2 and 2.0 ppm acetone,

respectively. Besides, the response and recovery times of S4 Au/In₂O₃ sensor were also further evaluated according to Fig. 6c. As shown in Fig. 6d, the dynamic processes become shortened with the increasing gas concentration, which may be due to lower gas concentration requires more time to reach equilibrium.

Table 1 A comparison of the performance of S1-S5 in this work

Samples	linear range (ppm)	response range	theory detection limit (ppb)
S1	0.1-50	1.2-14.9	120
S2	0.1-50	1.3-20.2	82
S3	0.2-50	2.5-53.9	51
S4	0.02-50	1.3-167.8	15
S5	0.05-50	1.4-80.0	35

Table 2 The response, detection limit, working temperature, response and recovery times of some typical semiconductor oxide based acetone gas sensors, and compared with that of S4 Au/In₂O₃ sensor in this work.

Sensing materials	Response (R _a /R _g)/corresponding concentration	Corresponding response in this work	Actual detection limit	Temp.	Res./Rec	Ref
S4 Au/In ₂ O ₃	42.4/5 ppm	42.4/5 ppm	20 ppb	340°C	~11/14 s	This work
ZnFe ₂ O ₄ nanospheres	12/30 ppm	22.3	800 ppb	200°C	~9/272 s	29
WO ₃ nanorods	3.1/0.5 ppm	10.2	0.25 ppm	230°C	~9/14 s	30
zeolite β modified ZnO	27/8 ppm	54.3	0.5 ppm	400°C	—	31
Ce-doped SnO ₂ hollow spheres	12/100 ppm	—	50 ppm	250°C	~18/7 s	32
5 mol% Cr ₂ O ₃ -doped WO ₃ films	9/20 ppm	96.1	0.5 ppm	320°C	~20/40 s	33
graphene-ZnFe ₂ O ₄ composite	3.5/10 ppm	63.5	<1 ppm	275°C	~4/18 s	34
porous spheres-like ZnO	20/2 ppm	26.0	—	310°C	3-4/4-5 s	35
ZnO nanorod arrays	20/8~9 ppm	~60	1 ppm	300°C	~5/15 s	36
Urchin-like ZnO nanorod arrays	246/100 ppm	—	—	300°C	—	37
SnO ₂ nanosphere functionalized TiO ₂	29/400 ppm	—	—	277°C	—	38
Pt-WO ₃ nanorod	1.27/0.3 ppm	7.5	0.3 ppm	350°C	—	39
Si-WO ₃ nanoparticle	4.6/0.6 ppm	11.6	20 ppb	400°C	~5.7/5.9 min	3
Cr-WO ₃ nanoparticle	1.5/0.2 ppm	5.9	—	400°C	~10/— s	40
Pt-WO ₃ hemitubes	1.3/0.12 ppm	3.8	120 ppb	300°C	—	41

More detail response data of S1-S5 3DIO sensors in the range of 0.02-50 ppm in their respective optimal operating temperature are shown in Fig. 7a. As can be seen, all the 3DIO sensors show clear responses signals to acetone gas in the range of their detection and the responses of all the IO sensors increase linearly with the increase of acetone concentration in log-log plot, indicating that this type sensor is very suitable for the detection of acetone in a wide range. The corresponding linear range, response ranges, and detection limit are listed in Table 1. Clearly, S4 Au/In₂O₃ sensor is still the best one, which has the widest linear ranges and 2.1-11.2 times higher response than the other IO sensors to 50 ppm acetone. Beyond that, the low detection limit of acetone of S4 Au/In₂O₃ sensor is deduced to be 15 ppb, which is 2.4-8.2 times lower than the other 3DIO sensors, when R_a/R_g ≥ 1.2 is used as the criterion for reliable gas sensing.²⁸ Table 2 listed the response, detection limit, working temperature, response and recovery times of some typical semiconductor oxide based acetone gas sensors, and compared with that of S4 Au/In₂O₃ sensor in this work. As can be seen, the sensor owns satisfied performance comparing to the other sensors, especially the response value and detection limit. Note that the actual low detection limit is 20 ppb for the S4 Au/In₂O₃ sensor, which is

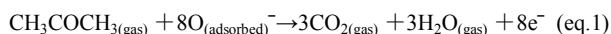
also much lower than the limits of detecting diabetes and some previous studies as listed in the Table 2. This confirms that the S4 Au/In₂O₃ sensor may be a promising candidate for monitoring of low concentration acetone biomarkers in exhaled breath.

Based on above sensing analysis, the clinic detection were applied to test the sensing performance of S4 Au/In₂O₃ sensor in human breath. As is known, the circumstance humidity is very high in exhaled breath. Here, the S4 Au/In₂O₃ sensor was explored to detect the acetone biomarker in exhaled breath samples, which were direct collection (100 RH%) and after dehumidification (20.0 RH%). The dehumidification of breath gas was removed by the gas-drying tube. The humidity was measured by the digital humidity and temperature meter (Hcjyet, HT-635). For the detection, 1 diabetic and 7 healthy volunteers participated in the test and the response data were shown in Fig. 8. The response data were obtained by sampling one time for each healthy volunteer and seven times for diabetic volunteer. The responses are about ~16 to diabetic, while ~25 to healthy person in untreated condition (Fig. 8a), and ~83 to diabetic, while ~42 to healthy person in dehumidified condition (Fig. 8b). As can be seen, the as fabricated sensor could identify the

diabetes patients from healthy people accurately. Besides, all the response values are higher in dehumidified condition than that in untreated condition. This can be ascribed to the fact that the surface active sites are occupied by heavy moisture which deteriorated the sensing performance. In dehumidified condition, the response values are higher compared to that in laboratory environment (Fig. 7), the reason can be attributed to the complex condition in exhaled breath, such as carbon dioxide, hydrothion, ketone et. al.

3.4 Gas sensing mechanism of 3DIO Au/In₂O₃ sensors

In₂O₃ is a typical n-type semiconducting sensor material, in which the key process of response to a reducing gas involves the concentration modulation of adsorbed oxygen species such as O²⁻, O⁻ or O²⁻, and the acetone gas sensing mechanism of In₂O₃ sensor can be explained by the surface-controlled model. In this mechanism, the resistance of In₂O₃ was controlled by the concentration of reactive oxygen species (O²⁻, O⁻ or O²⁻) that reacted with reductive acetone gas, resulting in the reduction of semiconductor conductivity. With the reaction of acetone and the reactive oxygen, the reactive oxygen concentration reduced and thereby the semiconductor conductivity increased. This reaction can be expressed as:



In this mechanism, the amount of active sites that could absorb the oxygen plays a very important role. When reducing gases are introduced, the reaction of the adsorb oxygen and the gas lead to the increase of the response. Thus, in our work, the calculated deficient oxygen ratios in different 3DIO sensors are consistent with the corresponding maximum response values in Fig. 5a, that is to say, the bigger the deficient oxygen ratios, the higher the response. Besides, with the increasing of the working temperature, the activation energy may also increase in the presence of In₂O₃ and/or Au and at the optimal working temperature, the activation energy may be just enough to complete the above chemical reaction.^{25, 26}

The improved sensing performance of the present 3DIO Au/In₂O₃ sensors may be attributed to three main aspects. When the introduced Au NPs are loaded on the 3DIO In₂O₃ samples, the “chemical sensitization” mechanism which is known as the “spillover effects” afforded by the metal NPs should be first considered (Scheme 1b).⁴² The Au is a far better oxygen dissociation catalyst than In₂O₃, which has high availability to catalytically active the dissociation of molecular oxygen, and then the as created activated oxygen species are spilled onto the metal oxides surface, thus more reactive oxygen species could be formed. This process has been considered to result in greater and faster reaction between analyses molecules and adsorbed oxygen (as proved by Fig. 5 and 6). In addition, ionsorption of oxygen ions occurred on the metal NPs surface at a low temperature (even at room temperature)⁴³ due to the highly conductive nature and availability of free electrons in Au. And that is why the optimal working temperature gradually decreased by increasing the amount of the surface coated Au NPs (Fig. 5a). However, when the loading of the Au is too much in our case (S5 gas sensor), heavy coating will deteriorate the 3DIO structure and the uniformity of the loading Au NPs, and thus has negative effect on gas sensing properties.

Second, the catalysis effect of Au should be considered due to noble metal can break hydrocarbons into more active radicals, the production of the reaction between surface adsorbed oxygen ions and the target gases is increased.²³ As shown in the energy band diagram of Au/In₂O₃ (Scheme 1b), because the different work function of Au (5.3 eV in our work) and In₂O₃ (5.1 eV in our work), the electrons in In₂O₃ will flow to Au, resulting in a Schottky barrier and an additional depletion layer at the interface at the Au/In₂O₃ interface. In acetone ambience, the electrons are released more easily from the surface reaction at the Au/In₂O₃ interface to the conduction band and consequently enhance the formation of electron charge transfer dynamics. Thirdly, the uniform 3DIO honeycomb-like structure with additional *via* holes around the order macroporous can provide high gas accessibility that let analyses gas molecules access readily and quickly, which make the sensors more active in gas detection.

4. Conclusions

To summarize, 3DIO In₂O₃ films with improved structure were first synthesized using a simple and modified sacrificial template method, and evaluated as chemiresistive acetone gas sensor towards diabetes biomarker in exhaled breath. Except regular honeycomb-like morphology, highly homogenous layout, 3DIO films also have uniform *via* holes in side pore around the order macroporous. Different amounts of Au NPs were uniformly interspersed on 3DIO In₂O₃ substrate, which enhanced the gas sensing performance effectively. A primary model was put forward to understand the growth mechanism of such improved structure. The comparative gas sensing tests exhibited that the sensing performance could be improved by pore size control and Au NPs loading. The S4 Au/In₂O₃ shows the best sensing behaviour, which has high response to trace acetone, low detection limited (15 ppb), much lower temperature compared to pure one, and good anti-interference. What's important, it can distinguish acetone biomarkers in human breath clearly. The improvement could be attributed to “spillover effects” as well as the unique feathers of unique 3DIO structure with additional *via* holes which can provide more reactive sites and high gas accessibility. Overall, we present a synthetic method for fabricating 3DIO structure with additional *via* holes, which is also applicable to other materials, and such structure could apply to a promising ppb-level acetone sensor for diabetes diagnosis through exhaled breath.

Acknowledgements

This work was supported by NSFC (Grant no. 61204015, 81301289, 61177042) Program for Chang Jiang Scholars and Innovative Research Team in University (No. IRT13018). The Jilin Province Natural Science Foundation of China (No. 20140101171JC). Project 2015021 Supported by Graduate Innovation Fund of Jilin University.

Additional information

Competing financial interests: The authors declare no competing financial interests.

References

1. M. Phillips, K. Gleeson, J. M. B. Hughes, J. Greenberg, R. N. Cataneo, L. Baker and W. P. McVay, *Lancet*, 1999, **353**, 1930.
2. G. Peng, U. Tisch, O. Adams, M. Hakim, N. Shehada, Y. Y. Broza, S. Billan, R. Abdah-Bortnyak, A. Kuten and H. Haick, *Nat. Nanotechnol.*, 2009, **4**, 669.
3. M. Righettoni, A. Tricoli and S. E. Pratsinis, *Anal. Chem.*, 2010, **82**, 3581.
4. H. Haick, Y. Y. Broza, P. Mochalski, V. Ruzsanyi and A. Amann, *Chem. Soc. Rev.*, 2014, **43**, 1423.
5. O. Barash, N. Peled, F. R. Hirsch and H. Haick, *Small*, 2009, **5**, 2618.
6. G. Konvalina and H. Haick, *Accounts Chem. Res.*, 2014, **47**, 66.
7. M. R. Alenezi, S. J. Henley, N. G. Emerson and S. R. P. Silva, *Nanoscale*, 2014, **6**, 235.
8. R. W. J. Scott, S. M. Yang, G. Chabanis, N. Coombs, D. E. Williams and G. A. Ozin, *Adv. Mat.*, 2001, **13**, 1468.
9. M. D'Arienzo, L. Armelao, A. Cacciamani, C. M. Mari, S. Polizzi, R. Ruffo, R. Scotti, A. Testino, L. Wahba and F. Morazzoni, *Chem. Mater.*, 2010, **22**, 4083.
10. H. Xu, P. Wu, C. Zhu, A. Elbaz and Z. Z. Gu, *J. Mater. Chem. C*, 2013, **1**, 6087.
11. L. Jia and W. Cai, *Adv. Funct. Mater.*, 2010, **20**, 3765.
12. M. D'Arienzo, L. Armelao, C. M. Mari, S. Polizzi, R. Ruffo, R. Scotti and F. Morazzoni, *J. Am. Chem. Soc.*, 2011, **133**, 5296.
13. Y. Xie, R. Xing, Q. Li, L. Xu and H. Song, *Sens. Actuators. B*, 2015, **211**, 255.
14. Z. Dai, C.-S. Lee, Y. Tian, I.-D. Kim and J.-H. Lee, *J. Mater. Chem. A*, 2015, **3**, 3372.
15. Z. Guo, J. Liu, Y. Jia, X. Chen, F. Meng, M. Li and J. Liu, *Nanotechnology*, 2008, **19**, 345704.
16. D. H. Zhang, Z. Q. Liu, C. Li, T. Tang, X. L. Liu, S. Han, B. Lei and C. W. Zhou, *Nano Letters*, 2004, **4**, 1919.
17. N. Singh, R. K. Gupta and P. S. Lee, *Acs Appl. Mater. Inter.*, 2011, **3**, 2246.
18. A. Gurlo, *Nanoscale*, 2011, **3**, 154.
19. Y. Zhu, W. Xu, H. Zhang, W. Wang, S. Xu and H. Song, *J. Phys. Chem. C*, 2012, **116**, 2297.
20. S. Y. Chou, P. R. Krauss and P. J. Renstrom, *Appl. Phys. Lett.*, 1995, **67**, 3114.
21. R.-q. Xing, L. Xu, Y.-s. Zhu, J. Song, W.-f. Qin, Q.-l. Dai, D.-l. Liu and H.-w. Song, *Sens. Actuators. B*, 2013, **188**, 235.
22. B. Erdem, R. A. Hunsicker, G. W. Simmons, E. D. Sudol, V. L. Dimonie and M. S. El-Aasser, *Langmuir*, 2001, **17**, 2664.
23. Q. Xiang, G. F. Meng, H. B. Zhao, Y. Zhang, H. Li, W. J. Ma and J. Q. Xu, *J. Phys. Chem. C*, 2010, **114**, 2049.
24. N. Du, H. Zhang, X. Ma and D. Yang, *Chem. Commun.*, 2008, **46**, 6182.
25. A. P. Lee and B. J. Reedy, *Sens. Actuators. B*, 1999, **60**, 35.
26. Z. A. Ansari, S. G. Ansari, T. Ko and J. H. Oh, *Sens. Actuators. B*, 2002, **87**, 105.
27. J. Mizsei, *Sens. Actuators. B*, 1995, **23**, 173.
28. C. W. Na, H.-S. Woo, I.-D. Kim and J.-H. Lee, *Chem. Commun.*, 2011, **47**, 5148.
29. X. Zhou, J. Liu, C. Wang, P. Sun, X. Hu, X. Li, K. Shimano, N. Yamazoe and G. Lu, *Sens. Actuators. B*, 2015, **206**, 577.
30. Q.-q. Jia, H.-m. Ji, D.-h. Wang, X. Bai, X.-h. Sun and Z.-g. Jin, *Journal Of Materials Chemistry A*, 2014, **2**, 13602.
31. D. C. Pugh, E. J. Newton, A. J. T. Naik, S. M. V. Hailes and I. P. Parkin, *J. Mater. Chem. A*, 2014, **2**, 4758-4764.
32. P. Song, Q. Wang and Z. Yang, *Sens. Actuators. B*, 2012, **173**, 839.
33. P. Gao, H. Ji, Y. Zhou and X. Li, *Thin Solid Films*, 2012, **520**, 3100.
34. F. Liu, X. Chu, Y. Dong, W. Zhang, W. Sun and L. Shen, *Sens. Actuators. B*, 2013, **188**, 469.
35. X. B. Li, S. Y. Ma, F. M. Li, Y. Chen, Q. Q. Zhang, X. H. Yang, C. Y. Wang and J. Zhu, *Mater. Lett.*, 2013, **100**, 119.
36. Y. Zeng, T. Zhang, M. Yuan, M. Kang, G. Lu, R. Wang, H. Fan, Y. He and H. Yang, *Sens. Actuators. B*, 2009, **143**, 93.
37. D. Barreca, D. Bekermann, E. Comini, A. Devi, R. A. Fischer, A. Gasparotto, C. Maccato, C. Sada, G. Sberveglieri and E. Tondello, *Crystengcomm*, 2010, **12**, 3419.
38. W. Zeng, T. Liu and Z. Wang, *J. Mater. Chem.*, 2012, **22**, 3544.
39. J. Shin, S.-J. Choi, D.-Y. Youn and I.-D. Kim, *J. Electroceram.*, 2012, **29**, 106.
40. L. Wang, A. Teleki, S. E. Pratsinis and P. I. Gouma, *Chem. Mater.*, 2008, **20**, 4794.
41. S.-J. Choi, I. Lee, B.-H. Jang, D.-Y. Youn, W.-H. Ryu, C. O. Park and I.-D. Kim, *Anal. Chem.*, 2013, **85**, 1792.
42. H. Wang, Z. Sun, Q. Lu, F. Zeng and D. Su, *Small*, 2012, **8**, 1167.
43. M. E. Franke, T. J. Koplín and U. Simon, *Small*, 2006, **2**, 36.